

The last migration trap of compact objects in AGN accretion disc

Peng Peng¹, Xian Chen^{1,2}★

¹*Astronomy Department, School of Physics, Peking University, 100871 Beijing, China*

²*Kavli Institute for Astronomy and Astrophysics at Peking University, 100871 Beijing, China*

Accepted XXX. Received YYY; in original form ZZZ

ABSTRACT

Many black holes (BHs) detected by the Laser Interferometer Gravitational-wave Observatory (LIGO) and the Virgo detectors are multiple times more massive than those in X-ray binaries. One possibility is that some BBHs merge within a few Schwarzschild radii of a supermassive black hole (SMBH), such that the gravitational waves (GWs) are highly redshifted, causing the mass inferred from GW signals to appear higher than the real mass. The difficulty of this scenario lies in the delivery of BBH to such a small distance to a SMBH. Here we revisit the theoretical models for the migration of compact objects (COs) in the accretion discs of active galactic nuclei (AGNs). We find that when the accretion rate is high so that the disc is best described by the slim disc model, the COs in the disc could migrate to a radius close to the innermost stable circular orbit (ISCO) and be trapped there for the remaining lifetime of the AGN. The exact trapping radius coincides with the transition region between the sub- and super-Keplerian rotation of the slim disc. We call this region “the last migration trap” because inside it COs can no longer be trapped for a long time. We pinpoint the parameter space which could induce such a trap and we estimate that the last migration trap contributes a few per cent of the LIGO/Virgo events. Our result implies that a couple of BBHs discovered by LIGO/Virgo could have smaller intrinsic masses.

Key words: stars: black holes – accretion discs – quasars: supermassive black holes – gravitational waves

1 INTRODUCTION

The binary black holes (BBHs) detected by the Laser Interferometer Gravitational-wave Observatory (LIGO) and the Virgo detectors (The LIGO Scientific Collaboration et al. 2020) are multiple times heavier than the black holes (BHs) detected previously in X-ray binaries (McClintock et al. 2014; Corral-Santana et al. 2016). Such a discrepancy has important implications for the formation and evolution of BHs (Abbott et al. 2016; The LIGO Scientific Collaboration et al. 2020; Abbott et al. 2020c, and the references therein). This remarkable discovery also excited interests to find alternative interpretations of the apparent high masses of the LIGO/Virgo BBHs.

There are at least two astrophysical scenarios in which the mass of a LIGO/Virgo BBH could be overestimated (see Chen 2020, for a review). Both scenarios are concerned with the effect of “mass-redshift degenerate”, i.e., from gravitational waves (GWs) only a redshifted mass $M(1+z)$ can be measured (Schutz 1986), where M is the intrinsic mass of the source and z is its redshift. The first scenario is related to gravitational lensing (Broadhurst et al. 2018; Smith et al. 2018). In this case, cosmological redshift causes the redshift of the mass, and lensing enhances the amplitude of the detected GW, which in turn reduces the apparent (luminosity) distance of the source. The large redshifted mass and the small apparent distance conspire to

result in an overestimation of the mass. However, this scenario has difficulty explaining all the heavy BBHs detected by LIGO/Virgo mainly because the lensing rate is relatively low (Hannuksela et al. 2019; LIGO Scientific Collaboration & Virgo Collaboration 2019; The LIGO Scientific Collaboration et al. 2020). The second scenario is concerned with the BBHs residing in the vicinity of supermassive black hole (SMBH). In this case, Doppler and gravitational redshifts predominate and cause the observed high mass (Chen et al. 2019). To gain a large redshift factor, the BBHs should form at a distance of a few Schwarzschild radii (r_s) from the central SMBH. One way of delivering BBHs to such a small distance is tidal capture but it has been shown that the event rate is also low (Addison et al. 2015; Chen & Han 2018).

There is an alternative way of forming BBHs close to a SMBH. It has been suggested that in active galactic nucleus (AGN), the accretion disc surrounding the central SMBH may contain a large amount of compact objects (COs), including stellar-mass BHs, neutron stars and white dwarfs. On one hand, the COs produced outside the accretion disc can be captured into it due to repeated collisions with the disc (Norman & Silk 1983; Syer et al. 1991; Artymowicz et al. 1993; MacLeod & Lin 2020; Davies & Lin 2020). On the other, massive stars can form in the outer, gravitationally unstable part of the accretion disc and end up as COs (Kolykhalov & Syun-yaev 1980; Shlosman & Begelman 1989; Goodman & Tan 2004; Levin 2007; Wang et al. 2010). Once in the accretion disc, COs

★ E-mail: xian.chen@pku.edu.cn

could form binaries efficiently by giving away excessive energy and angular momentum to the surrounding gas (McKernan et al. 2012; Secunda et al. 2019; Tagawa et al. 2020). Moreover, the interaction with the gas (Baruteau et al. 2011; Bartos et al. 2017; Stone et al. 2017) and the other COs in the disc (Leigh et al. 2018; Yang et al. 2019), or even the SMBH (Antonini et al. 2014), also accelerates the coalescence of the binaries. As a result, the merger rate of the COs in AGN accretion discs could be significant. For example, recent calculations suggest that the merger rate of the BBHs in AGN discs could be as high as $10 - 10^2 \text{ Gpc}^{-3} \text{ yr}^{-1}$ (McKernan et al. 2018; Antoni et al. 2019; Secunda et al. 2020; Gröbner et al. 2020; Tagawa et al. 2020). Interestingly, it is reported that GW190521—the most massive LIGO BBH—has an AGN counterpart (Graham et al. 2020).

If an AGN disc contains a large amount of BHs, it is natural to conjecture that a fraction of them may migrate to a small distance of $\lesssim 10r_s$ from the central SMBH due to hydrodynamical torque (known as “type I migration”, Goldreich & Tremaine 1979, 1980; Ward 1991; Yunes et al. 2011; Kocsis 2013; Barausse et al. 2014). Consequently, BBHs may form there and produce seemingly overweight LIGO/Virgo BBHs, due to the large Doppler and gravitational redshift (Chen et al. 2019). However, an earlier work shows that there are places outside a radius of $10^2 r_s$ where the positive and negative gas torques cancel out (Bellovary et al. 2016). As a result, the migration halts and BHs would be trapped there. Although these “migration traps” are favorable places for BBH formation (Secunda et al. 2019; Yang et al. 2019; Secunda et al. 2020), they are too far from the central SMBH to induce any significant redshift effect.

Recently, Pan & Yang (2021) considered the effect of the thickness of AGN accretion disc and found that the COs embedded in thick discs could overcome the migration traps. Their scenario is in close analogy with the migration of planetesimals in protoplanetary discs. It is well known that protoplanetary discs are rotating slower than the Keplerian velocity because they are partially supported by gas pressure (Weidenschilling 1977). In particular, the deviation from Keplerian rotation increases as the disc becomes thicker, because thicker discs have higher pressure. Planetesimals, on the contrary, are less affected by the gas pressure and are moving with Keplerian velocities. The difference in velocity induces effectively a headwind on the planetesimals, which drives the planetesimals to migrate inward (Adachi et al. 1976; Ward 1997; Weidenschilling & Cuzzi 1993; Youdin & Shu 2002). The headwind mechanism also applies to AGN discs, and according to Pan & Yang (2021) it is so efficient that the BHs in the accretion disc always feel a negative torque so that they will quickly migrate to the innermost stable circular orbit (ISCO) of the central SMBH.

The behaviour of COs close to the ISCO of AGN accretion disc has been studied in the early works of Chakrabarti (1993, 1996); Molteni et al. (1994). Interestingly, they revealed that in some cases the COs will, again, be trapped. It happens in a region close to the ISCO where the gas rotates faster than the Keplerian velocity. Such a super-Keplerian motion is the result of a generic relativistic effect which causes the pressure gradient to point inward to the SMBH (Abramowicz et al. 1978, 1988; Lančová et al. 2019). Since now the COs rotate slower than the gas because their rotation velocity is Keplerian, they will feel a tailwind and gain angular momentum. In the original proposal of Chakrabarti (1993), the tailwind counteracts the negative torque caused by the GW radiation of the CO-SMBH binary, and hence it will halt the inward migration of the CO. We refer to this place as the “last migration trap” because inside it there is no more place where COs can be trapped.

These previous works point to a picture that the COs in an

AGN accretion disc would be flushed, due to the headwind, to a place close to the ISCO and then be trapped there, as a result of a flip of the direction of the wind. Because of their closeness to the central SMBH, the GW sources forming in this last migration trap will be affected by significant Doppler and gravitational redshift. As a first step towards understanding the merger rate of the COs inside the last migration trap, in this paper we build an accretion disc model which self-consistently generates the rotation velocity of the gas, especially the transition from sub-Keplerian to super-Keplerian rotation. We analytically study the migration of COs in such a disc and identify the parameter space where the last migration trap exists.

The paper is organized as follows. In Section 2, we describe our disc model and lay out our scheme of calculating the drag force imposed on the CO. In Section 3, we derive the migration time-scale of a CO in the aforementioned disc and look for the parameter space where the last migration trap exists. We discuss in Section 4 the limitation of our analytical method as well as the implications for future GW observations.

2 MODELS

2.1 Slim disc model

The accretion disc of our interest should have a mild thickness, to induce a non-Keplerian rotation. It should also have a relatively high density so as to capture or form COs in it. Since we are interested in the region close to the SMBH, we need to consider advective cooling because radiation becomes insufficient to cool the disc. These conditions are satisfied in the slim disc model. This model was constructed first assuming a pseudo-Newtonian potential (Abramowicz et al. 1988) and later with general relativistic corrections (Abramowicz et al. 1996, 1997; Beloborodov 1998; Sądowski 2009; Sądowski 2011). Because of the relativistic corrections, the transition of the inner disc from sub-Keplerian to super-Keplerian rotation can be self-consistently modeled. Since we need an accurate disc profile extending to $r \lesssim 10r_s$ to perform our calculation, we adopt the full general relativistic disc model as is described in Section 4 of Sądowski (2011).

The slim disc model adopted by us is governed by six equations. Four of them are the same as the relativistic standard disc (Novikov & Thorne 1973), namely, the equations for mass conservation, angular momentum conservation, vertical equilibrium and the equation of state. The fifth equation is for energy conservation. Besides the normal terms of viscous heating and radiative cooling, there is an extra term representing advection. The last equation is for momentum conservation in the radial direction. It contains both the pressure gradient and the radial velocity gradient. When they become large, the actual angular velocity of the disc, Ω , would deviate from the Keplerian angular velocity, Ω_k . The departure from Keplerian motion gives rise to the headwind and tailwind, which will act on the COs and affect their migration in the accretion disc.

We simplify the disc model in two aspects so that we can perform the later calculation relatively quickly. First, we assume that the central SMBH is not spinning. This assumption will increase the transition radius between sub-Keplerian and super-Keplerian rotation, but the disc remains non-Keplerian (Sądowski 2009; Sądowski 2011). Since the transition radius determines the location of the last migration trap, our model would overestimate the trapping radius for COs and subsequently lead to a conservative estimation of the redshift effect. The second simplification is that we replace

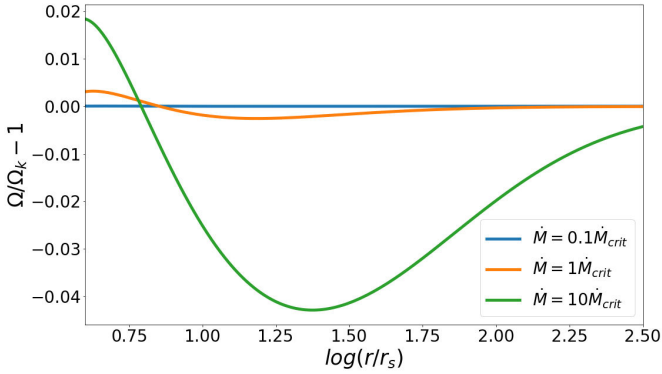


Figure 1. The difference between the actual angular velocity of the gas Ω and the Keplerian angular velocity Ω_k as a function of radius. In this example, the mass of the SMBH is $10^8 M_\odot$ and the viscosity parameter is $\alpha = 0.01$. The blue, orange and green lines correspond, respectively, to an accretion rate of $\dot{M} = 0.1, 1$ and $10 \dot{M}_{\text{crit}}$.

the vertical integration of gas density and pressure with a simple multiplication of the height H of the disc. Although this simplification changes the corresponding terms by a constant coefficient, it preserves the main feature of the slim disc, i.e., the disc remains thickness and has a large pressure gradient.

There is no analytical solution to our slim disc model because there is an eigenvalue, the specific angular momentum at the sonic point, which is not known *in pri ori* and has to be determined numerically (Sadowski 2011). In our work, we find this eigenvalue by integrating the disc out-side-in, starting from the outer boundary whose physical conditions are set by the standard disc (Kato et al. 2008).

Using this model, we can solve the disc structure for a SMBH in the mass range of $M_{\text{SMBH}} = 10^5 - 10^9 M_\odot$ with an accretion rate of $\dot{M} = 0.1 - 10 \dot{M}_{\text{crit}}$, where \dot{M}_{crit} is the critical accretion rate defined as $16L_{\text{Edd}}/c^2$ (Sadowski 2011) with L_{Edd} being the Eddington luminosity. We also try different values for the viscosity parameter α , ranging from 0.01 to 0.1. Given a set of parameters, we solve the equations in the radial range between $r = 10^4 r_s$ and $3 r_s$.

Figure 1 shows the difference between the angular velocity derived from our slim disc model and the Keplerian angular velocity. Here we fix the mass of the SMBH to $M_{\text{SMBH}} = 10^8 M_\odot$ as well as the viscous parameter to $\alpha = 0.01$, and we vary the accretion rate between $\dot{M} = 0.1 \dot{M}_{\text{crit}}$ and $10 \dot{M}_{\text{crit}}$. When $\dot{M} = 0.1 \dot{M}_{\text{crit}}$, the angular velocity is close to Keplerian throughout the disc. With higher accretion rate, the deviation from the Keplerian velocity becomes more prominent and could be several per cent at $r < 100 r_s$. For all the three accretion rates, the discs are sub-Keplerian at $r \gtrsim 10 r_s$ and super-Keplerian at $r \lesssim 10 r_s$. Such a transition will be important for our later study of the trapping radius of COs. For other values of M_{SMBH} and α , the angular velocity profiles have a similar behaviour and hence are not shown here.

2.2 Drag force model

Unlike gas, COs around a SMBH are not significantly affected by the radial pressure gradient of the disc. Therefore, their rotation velocities remain Keplerian. Now that the COs are moving at a velocity different from the velocity of the gas, they will feel a wind. In the sub-Keplerian region of the accretion disc, such as the outer

part of the disc, a CO will encounter a headwind (Pan & Yang 2021), and in the super-Keplerian region, such as the inner part of the disc, it will feel a tail wind (Chakrabarti 1993). In either case, the wind would induce an effective drag force on the CO (see e.g. Pan & Yang 2021, for discussion). The difference is that the headwind drags the CO backward and extracts angular momentum from the orbit, while the tailwind pushes the CO forward and imparts angular momentum to the CO. Previous works considered the headwind and tailwind separately (Chakrabarti 1993; Pan & Yang 2021), but here we will include both effects in our model. The inclusion of both types of winds, as well as the torque corresponding to GW radiation (see the next section), will allow us to pin down the location where the net torque vanishes. Such a location would be our last migration trap.

One essential ingredient that differentiates our model from the previous ones is a mini accretion disc around the CO. Presence of the mini disc is a natural consequence of the conservation of angular momentum, and earlier numerical simulations suggest that its size could be as large as the Hills radius $R_H = q^{1/3} r_0$ (Lin & Pringle 1976; Artymowicz & Lubow 1994; Baruteau et al. 2011), where $q = M_{\text{CO}}/M_{\text{SMBH}}$ is the mass ratio between the CO and the SMBH, and r_0 denotes the orbital radius of the CO around the SMBH. The mini disc significantly enhances the interaction cross section of the CO with the gas in the AGN disc, because any fluid parcel crossing the mini disc would exchange momentum with the CO. For example, in the conventional scenario of Bondi-Hoyle-Lyttleton accretion the cross section of exchanging momentum is determined by $\Sigma_{\text{BHL}} \sim G^2 M_{\text{CO}}^2 / (V_{\text{rel}}^2 + c_s^2)^2$, where V_{rel} is the relative velocity between the CO and the gas in the surrounding AGN disc, and c_s is the sound speed of the gas. Comparing it to the physical cross section of the Hills sphere, $\Sigma_H \sim R_H^2$, we find that

$$\frac{\Sigma_H}{\Sigma_{\text{BHL}}} \gtrsim \left(\frac{M_{\text{SMBH}}}{M_{\text{CO}}} \right)^{4/3} \left(\frac{H}{r_0} \right)^4, \quad (1)$$

where we have used the condition of hydrostatic equilibrium, $c_s \approx \Omega_k(H/r_0)$. In this work, typically, $(H/r_0) \sim 0.1$ for $\dot{M} = 1 \dot{M}_{\text{crit}}$. So the above ratio is significantly greater than unity in the slim disc region where H is not much smaller than r_0 . This result indicates that we have to consider the interaction between the mini disc and the fluid in the AGN accretion disc so as to properly account for the drag force imposed on the CO.

Following the above scenario, we now calculate the drag force exerted on the mini disc. The CO feels the same force because of a strong gravitational coupling between the mini disc and the CO (e.g. see Chen et al. 2020, for a discussion). Without loss of generality, we write the momentum flux imparted onto the mini disc as

$$F_{\text{gas}} = k \rho(r_0) R_H^2 V_{\text{rel}}^2, \quad (2)$$

where $\rho(r_0)$ is the unperturbed gas density in the AGN accretion disc, evaluated at the orbital radius r_0 of the CO. The geometrical coefficient k depends on the actual velocity field of the gas around the CO and will be determined later. In principle it is of order unity because the size of the Hills sphere sets a characteristic cross section for gas-disc interaction. The direction of the drag force is the same as the velocity of the gas relative to the CO, because it is the direction where momentum is added to the mini disc. Note that using our notation, the relative velocity is $V_{\text{rel}} = [\Omega(r_0) - \Omega_k(r_0)] r_0$.

To determine the geometrical factor k , we have to first understand the velocity field of the gas around the CO. We notice that previous works only considered a single value for the relative velocity between the CO and the gas (Chakrabarti 1993; Pan & Yang 2021), which is the aforementioned V_{rel} . This approximation

is valid in the region where differential rotation of the AGN accretion disc is negligible (see the left panel of Figure 2). In our case, since the CO is relatively close to the SMBH ($\lesssim 10^2 r_s$) and the differential rotation velocity increases with decreasing r_0 , we have to consider a variation of V_{rel} across the characteristic scale of the mini disc. Now consider a fluid element in the AGN accretion disc which has an initial orbital radius $\delta r + r_0$, where $|\delta r| \ll r_0$ for our problem. Its orbital velocity is $(\delta r + r_0)\Omega(\delta r + r_0) \approx r_0\Omega(r_0) + d[r\Omega(r)]/dr \delta r \approx \Omega(r_0)r_0 - \Omega(r_0)\delta r/2$, where we have assumed that $\Omega(r)$ does not significantly deviate from $\Omega_k(r)$, which is valid according to Figure 1. Therefore, the velocity relative to the CO is $V_{\text{rel}}(r_0) - \Omega(r_0)\delta r/2$, where the first term comes from the non-Keplerian motion of the fluid and the second term from the differential rotation. As is illustrated in the right panel of Figure 2, the differential rotation could even flip the direction of V_{rel} across a radial scale of R_H if r_0 is small. Consequently, different parts of the mini disc feels different types of wind. The headwind and tailwind, combined, give rise to a net force acting on the CO.

Knowing the velocity field of the gas, we now proceed to determine which part could enter the Hills radius and fuel the mini disc. Here we cannot use the standard formula for gravitational focusing because the background is not flat—it is determined by the tidal field of the SMBH. Instead, we use the “impulse model” (Armitage 2010). According to this model, when a fluid element passes by the CO, the gravitational force of the CO on the fluid element is the strongest within the time interval $\delta t = 2|\delta r|/|V_{\text{rel}}(r_0) - \Omega(r_0)\delta r/2|$. During this time interval, the velocity of the fluid element changes by $\delta v \sim \delta t GM_{\text{CO}}/\delta r^2$. Such a velocity change will excite the orbital eccentricity of the fluid element to a value of $\delta v/(\Omega r)$. If this orbital eccentricity falls in the range of $|\delta r \mp R_H|/r_0$, the fluid element could reach the mini disc and is in the so-called “feeding zone”. Following this argument, we find that the boundaries of the feeding zone satisfy the equation

$$4GM_{\text{CO}} = \pm \Omega^2 \delta r^3 \mp 2V_{\text{rel}}\Omega\delta r^2 - R_H\Omega^2\delta r^2 + 2R_HV_{\text{rel}}\Omega\delta r, \quad (3)$$

where plus and minus signs correspond to gas moving in opposite directions relative to the CO. One can verify the above equation by considering a Keplerian disc, i.e., in the case where the second and fourth terms on the right hand side vanish. One will recover the result that the boundaries of the feeding zone are at $\delta r_{\pm} = \pm 2R_H$ (Armitage 2010). For our non-Keplerian disc, the second and fourth terms on the right hand side of Equation (3) do not vanish. However, they are small relative to the first and third terms so that we can expand δr to the order of $V_{\text{rel}}/\Omega(r_0)$ and derive $\delta r_{\pm} = \pm 2R_H + V_{\text{rel}}/2\Omega(r_0)$. Not all the gas within the above boundary can interact with the mini disc. Some fluid elements are on the so-called “horseshoe orbit” which does not enter the Roche radius of the CO (Ward 1991). Here we follow the treatment used in Armitage (2010) and assume that the width of the feeding zone is half of the width of the boundaries.

Now we know the width of the feeding zone ($|\delta r_{\pm}|/2$) and the velocity field in it ($V_{\text{rel}}(r_0) - \Omega(r_0)\delta r/2$), we can calculate the momentum flux deposited onto the mini disc and derive the drag force exerted on the CO. Assuming that the height of the feeding zone is $|\delta r_{\pm}|/2$ (Armitage 2010), we find that the drag force (to the lowest order of $V_{\text{rel}}/\Omega R_H$) is

$$\begin{aligned} F_{\text{gas}} &= -\rho(r_0)(V_{\text{rel}} - \Omega(r_0)\delta r_+/2)^2\delta r_+^2/4 \\ &\quad + \rho(r_0)(V_{\text{rel}} - \Omega(r_0)\delta r_-/2)^2\delta r_-^2/4 \\ &= -\rho\Omega^2(r_0)[R_H - 3V_{\text{rel}}/4\Omega(r_0)]^2[R_H + V_{\text{rel}}/4\Omega(r_0)]^2 \\ &\quad + \rho\Omega^2(r_0)[R_H + 3V_{\text{rel}}/4\Omega(r_0)]^2[R_H - V_{\text{rel}}/4\Omega(r_0)]^2 \\ &\sim \rho R_H^3\Omega(r_0)[\Omega(r_0) - \Omega_k(r_0)]r_0. \end{aligned} \quad (4)$$

The direction of the force is also the same as $V_{\text{rel}}(r_0)$. Therefore, the CO feels a headwind (tailwind) if it resides in the sub-Keplerian (super-Keplerian) region of the disc.

We can unify the Equations (2) and (6) by writing the drag force as

$$F_{\text{gas}} = k\rho(r_0)R_H^2[\Omega(r_0) - \Omega_k(r_0)]^2r_0^2, \quad (7)$$

where $k = \max[1, \Omega(r_0)R_H/(|\Omega(r_0) - \Omega_k(r_0)|r_0)]$. We can see that when the differential rotation is unimportant, i.e., $\Omega(r_0)R_H < |\Omega(r_0) - \Omega_k(r_0)|r_0$, we have $k = 1$ and we recover Equation (2). On the contrary, if the differential rotation is not negligible, i.e., $\Omega(r_0)R_H > |\Omega(r_0) - \Omega_k(r_0)|r_0$, we have $k = \Omega(r_0)R_H/|\Omega(r_0) - \Omega_k(r_0)|r_0$ and Equation (6) is recovered.

We note that the derivation of the drag force assumes that $R_H < H$. This assumption is valid because in our model $R_H/H = (r_0/H)(M_{\text{CO}}/M_{\text{SMBH}})^{1/3}$. Note that the thickness of the disc is related to the non-Keplerian motion of the disc (see Figure 1) as

$$\left(\frac{H}{r_0}\right)^2 \approx 2\left|\frac{\Omega}{\Omega_k} - 1\right| \quad (8)$$

according to Equations (4.7), (4.10) and (4.12) of Sadowski (2011) in the non-relativistic limit, which, in turn, is related to the accretion rate. For example, we find that $H/r \sim 0.01, 0.1, 0.3$ at $r < 100 r_s$, when the accretion rate is $\dot{M} = 0.1, 1, 10 \dot{M}_{\text{crit}}$. As a result, the value of R_H/H is smaller than 1 in the region of $r_0 \lesssim 10^2 r_s$ around the SMBHs of our interest ($M_{\text{SMBH}} \gtrsim 10^7 M_{\odot}$).

We also note that we can neglect the drag force induced by the radial advection of the slim disc because it is much weaker than the centrifugal force. The force exerted by the radial advection on the mini disc can be estimated with $\rho R_H^2 V_r^2$, where V_r is the radial velocity of the gas. The centrifugal force is $M_{\text{CO}}\Omega_k^2 r_0$. The ratio of the two forces is:

$$\frac{\rho R_H^2 V_r^2}{M_{\text{CO}}\Omega_k^2 r_0} = q^{-1/3} \frac{V_r^2}{\Omega_k^2 r_0^2} \frac{\rho r_0^3}{M_{\text{SMBH}}} \sim q^{-1/3} \alpha^2 \left(\frac{H}{r_0}\right)^3 \frac{\Sigma r_0^2}{M_{\text{SMBH}}}, \quad (9)$$

where $\Sigma \sim H\rho$ is the surface density of the disk and we have used $V_r = \alpha H^2 \Omega_k^2$ based on the equations of mass conservation and angular momentum conservation. With typical parameters in this work ($q \geq 10^{-8}$, $\alpha \leq 0.1$, $H/r_0 \lesssim 0.3$, $\Sigma r_0^2/M_{\text{SMBH}} \lesssim 10^{-4}$), we find that the drag force induced by the radial advection is negligible.

3 RESULTS

Given the disc and drag force models, we can study the migration of COs in our non-Keplerian disc. We first compare four characteristic time-scales which outline the behavior of a CO in AGN disc. These four time-scales are (i) the migration time-scale T_{gas} due to the interaction with the headwind/tailwind, (ii) type I migration time-scale T_I as has been studied extensively in the previous works on COs in AGN discs (e.g. Bellovary et al. 2016), (iii) orbital decay time-scale of the CO due to GW, T_{GW} , which becomes particularly important at small radius r_0 and (iv) the lifetime of the AGN T_{AGN} . In general, the shortest time-scale of T_{gas} , T_I and T_{GW} determines which mechanism drives the migration of COs. However, if T_{AGN} becomes the shortest time-scale, the accretion disc would disappear and the migration of CO would stall. In this case a CO cannot reach a close distance to the central SMBH.

To calculate T_{gas} , we use Equation (7) and write

$$T_{\text{gas}} = \frac{M_{\text{CO}}\Omega_k r}{F_{\text{gas}}} = k^{-1} q^{1/3} \frac{\Omega_k^2}{(\Omega - \Omega_k)^2} \frac{M_{\text{SMBH}}}{\rho r^3} \frac{1}{\Omega_k}. \quad (10)$$

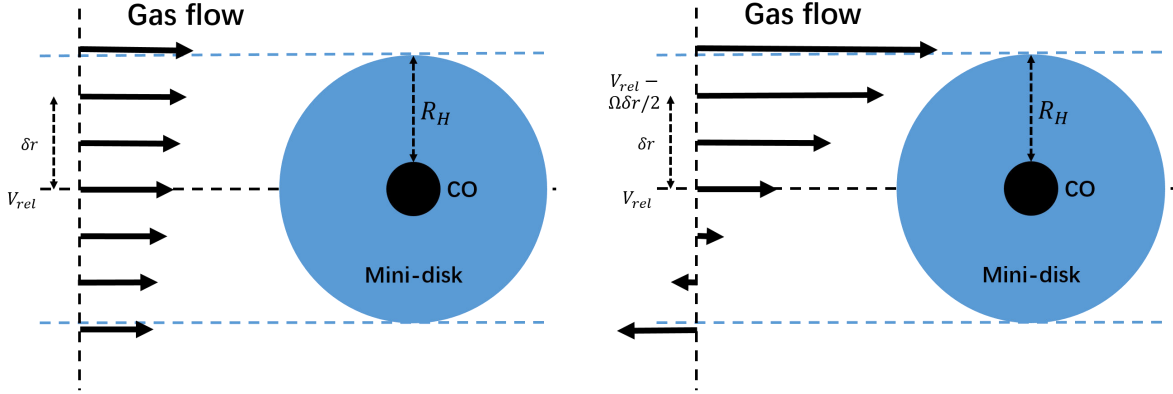


Figure 2. Sketch of the mini-disc of a CO and the velocity field of the incoming gas flow. The vertical direction coincides with the radial direction of the AGN disc. The horizontal arrows indicate the direction and magnitude of the relative velocity between the gas flow and the CO. The left panel shows the case in which the differential rotation of the AGN accretion disc is small, so that the velocity of the gas relative to the CO is more or less constant across the surface of the mini disc. This case corresponds to a large distance between the CO and the SMBH. The right panel shows the case where the differential rotation of the AGN accretion disc is significant. The CO in this case is close to the SMBH.

Using the relationship derived in Equation (8) and the approximation that $\rho \sim \Sigma/H$, we can derive a more quantitative equation for T_{gas} as

$$T_{\text{gas}} = 4k^{-1}q^{\frac{1}{3}}\left(\frac{H}{r}\right)^{-3}\frac{M_{\text{SMBH}}}{\Sigma r^2}\frac{1}{\Omega_k} = 0.18\text{Myr}k^{-1}\left(\frac{M_{\text{CO}}}{10M_{\odot}}\right)^{\frac{1}{3}} \\ \times \left(\frac{M_{\text{SMBH}}}{10^8M_{\odot}}\right)^{-\frac{4}{3}}\left(\frac{r}{10r_s}\right)^{-\frac{3}{2}}\left(\frac{H}{r}\right)^{-3}\left(\frac{\Sigma}{10^5\text{g cm}^{-2}}\right)^{-1} \quad (11)$$

In the last equation we have chosen the typical values of M_{CO} , M_{SMBH} and Σ for scaling. We note that depending on the direction of the wind, the CO would migrate either inward or outward on the time-scale of T_{gas}

Type I migration is caused by the interaction between the CO and the density waves in the disc (Goldreich & Tremaine 1980). The direction of the migration, as is noted in the earlier work of migration trap (Bellovary et al. 2016), could be either inward or outward depending on the exact temperature and density profiles of the accretion disc. We follow Ward (1997) and calculate the corresponding time-scale as

$$T_I = q^{-1}\frac{M_{\text{SMBH}}}{\Sigma r^2}\frac{1}{\Omega_k}. \quad (12)$$

Compare it with the time-scale due to gas drag, we find that

$$T_{\text{gas}}/T_I = 4k^{-1}q^{1/3}\left(\frac{H}{r}\right)^{-3}\frac{M_{\text{SMBH}}}{\Sigma r^2}\frac{1}{\Omega_k}\left/q^{-1}\frac{M_{\text{SMBH}}}{\Sigma r^2}\frac{1}{\Omega_k} \quad (13) \\ = 4q^{4/3}(H/r)^{-5} = 0.6\left(\frac{M_{\text{CO}}}{10M_{\odot}}\right)^{4/3}\left(\frac{M_{\text{SMBH}}}{10^8M_{\odot}}\right)^{-4/3}\left(\frac{H/r}{0.02}\right)^{-5}. \quad (14)$$

Apparently, type I migration becomes less efficient than the gas drag as the mass of the CO decreases. Besides, a heavier SMBH or a thicker accretion disc could also suppress the relative importance of type I migration. For these reasons, in the following analysis we focus on the cases in which $M_{\text{SMBH}} \gtrsim 10^7M_{\odot}$, $M_{\text{CO}} \lesssim 100M_{\odot}$ and $H/r \gtrsim 0.01$. The last condition about the disc scale height corresponds to an accretion rate of $\dot{M} \gtrsim 0.1\dot{M}_{\text{crit}}$.

As the CO is driven closer to the SMBH, the GW radiation of the SMBH-CO system becomes more powerful and needs to be accounted for in the calculation of the migration time-scale. The orbital decay time-scale due to GW radiation can be calculated with

$$T_{\text{GW}} = \frac{5c^5r^4}{256G^3(M_{\text{SMBH}} + M_{\text{CO}})M_{\text{SMBH}}M_{\text{CO}}} \quad (15)$$

(Peters 1964). It follows that

$$\frac{T_{\text{gas}}}{T_{\text{GW}}} = \frac{128\sqrt{2}}{5}q^{4/3}(1+q)\frac{M_{\text{SMBH}}}{\Sigma r^2}\left(\frac{H}{r}\right)^{-3}\left(\frac{r}{r_s}\right)^{-5/2} \quad (16) \\ = 1.2\left(\frac{M_{\text{CO}}}{10M_{\odot}}\right)^{\frac{4}{3}}\left(\frac{M_{\text{SMBH}}}{10^8M_{\odot}}\right)^{-\frac{10}{3}}\left(\frac{r}{10r_s}\right)^{-\frac{11}{2}} \\ \times \left(\frac{H/r}{0.1}\right)^{-3}\left(\frac{\Sigma}{10^5\text{g cm}^{-2}}\right)^{-1}. \quad (17)$$

Equation (17) shows that at a close distance $r \sim 10r_s$, where the AGN accretion disc is thick and super-Keplerian, the migration time-scale due to gas drag T_{gas} could be comparable to the GW radiation time-scale T_{GW} , provided that the CO is small and the SMBH is massive. In this case, the gas gives angular momentum to the CO at a rate comparable to the rate the GW radiation extracts angular momentum from the CO. As a result, the CO stalls at such a small radius.

Such a stalling radius is absent in the work of Pan & Yang (2021), because they did not use the slim disc model so that their disc lacks a super-Keplerian inner region. Our stalling radius is also different from what have been found by Chakrabarti (1993); Molteni et al. (1994) because we consider a mini disc surrounding the CO. The mini disc taps more angular momentum from the tailwind, and hence results in a smaller stalling radius than what Chakrabarti (1993); Molteni et al. (1994) have predicted.

The lifetime of AGN determines how long an accretion disc is present around the SMBH. We are interested in a particular phase of AGN during which the accretion rate is higher than $\dot{M} \gtrsim 0.1\dot{M}_{\text{crit}}$. We denote the duration of such a phase as T_{AGN} . After this phase, the disc is geometrically thin and the super/sub-Keplerian motion of the gas becomes less prominent. However, it is challenging to predict the value of T_{AGN} (Shankar et al. 2009). This is so because observations show that AGNs vary significantly on different time-scales, from several days (Caplar et al. 2017) to less than 1 Myr (Schawinski et al. 2015; Sartori et al. 2018), and even as long as several hundred Myrs (Gonçalves et al. 2008). In this work, for simplicity we assume that $T_{\text{AGN}} = 10^7$ yrs. It is a typical value for

high luminosity AGNs (Gonçalves et al. 2008; Hopkins & Hernquist 2009; Gabor & Bournaud 2013). Since it is shorter than the Salpeter time-scale $T_{\text{Sal}} = 3 \times 10^7 (\dot{M}_{\text{crit}}/\dot{M}) \text{ yrs}$ (Salpeter 1964) unless \dot{M} is significantly greater than $3\dot{M}_{\text{crit}}$, we will neglect the variation of the mass of the SMBH in our model.

For massive COs, type II migration also becomes important (Lin & Papaloizou 1986). This type of migration requires that the CO opens a gap in the AGN accretion disc due to tidal interaction. After the gap forms, the migration of the CO is driven mainly by the torque exerted by the density waves at the edges of the gap. For a CO in a Keplerian thin disc, it can be shown that the type II migration time-scale is short, of the order of $T_{\text{Sal}} (M_{\text{CO}}/M_{\text{SMBH}})$ (e.g. Chen et al. 2020). Therefore, the CO could migrate inward efficiently. For slim discs, however, radial advection becomes important in the transportation angular momentum, but there is no analytical or numerical calculation of the gap formation and migration time-scales. For this reason, in this work we do not consider the COs undergoing type II migration. In practice, we check the criteria for gap opening

$$\frac{R_{\text{H}}}{H} \left(\frac{8H/r}{27\pi\alpha} \right)^{1/6} > 1 \quad \text{or} \quad \frac{R_{\text{H}}}{H} \left(\frac{H/r}{1600\alpha} \right)^{1/3} > 1. \quad (18)$$

(Lin & Papaloizou 1986; Bryden et al. 1999), and stop the calculation when these criteria are met.

Although the time-scales T_{gas} , T_{I} and T_{GW} derived above are informative about the efficiencies of different migration types, they do not show the directions of the migration. Therefore, we further derive the torque exerted on the CO, to show both the magnitude and the direction of the corresponding effect. In the following, a positive torque drives the CO outward and a negative one drives it inward. The torque due to the headwind/tailwind can be written as $\Gamma_{\text{gas}} = F_{\text{gas}} r$, where the direction is determined by the sign of the force F_{gas} . For Type I migration, the torque Γ_{I} is calculated as in Paardekooper et al. (2010). For GW radiation, the torque Γ_{GW} is always negative and has been derived in Peters (1964). The sum of the torques, $\Gamma_{\text{sum}} = \Gamma_{\text{gas}} + \Gamma_{\text{I}} + \Gamma_{\text{GW}}$, determines the final direction of the migration.

Figure 3 shows the values of Γ_{gas} , Γ_{I} , Γ_{GW} and Γ_{sum} at different radius of the AGN accretion disc. In the calculation we have assumed that $M_{\text{CO}} = 10 M_{\odot}$, $M_{\text{SMBH}} = 10^9 M_{\odot}$ and $\dot{M} = 1\dot{M}_{\text{crit}}$. These torques are normalized by $10^{-10} M_{\text{CO}} c^2$. The upper panel shows the torques which drive the COs outward and the lower one shows the torques which drive the COs closer to the SMBH. In both panels, we find that the torque Γ_{gas} due to headwind/tailwind predominates. In particular, at $r \gtrsim 30 r_s$, the negative gas drag torque (orange curve) overcomes the positive, type I migration torque (blue curve). This result indicates that the headwind could push the COs out of the migration traps and force them to migrate closer to the SMBH. The same result was derived recently by Pan & Yang (2021), who used a different accretion disc model and did not consider the effects of the mini disc. Our result complements theirs and supports their conclusion that the type I migration traps as is envisioned in Bellovary et al. (2016) may not exist in thick discs.

However, Figure 3 reveals a new kind of migration trap at a small radius of $r \sim 7 r_s$ (see the dashed vertical line on the left). Here the gas drag (orange curve) still predominates. Nevertheless, the total torque (orange curve) changes sign because the accretion flow transforms from sub-Keplerian to super-Keplerian, i.e., the wind direction changes. COs could be trapped here because at $r \gtrsim 7 r_s$ the total torque is negative, forcing the COs to migrate inward, and at $r \lesssim 7 r_s$ the total torque becomes positive, forcing the COs to migrate outward. This trap is characteristically different from the type I mi-

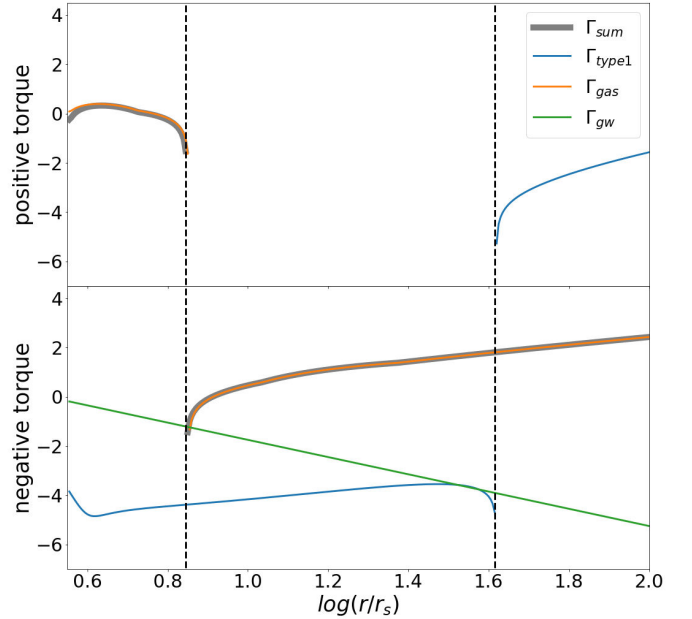


Figure 3. Different types of torques as a function of the distance from the central SMBH. The blue, orange, green and grey curves represent the torques due to Type I migration, headwind/tailwind, GW radiation and the sum of the previous three. The unit of the torque is $10^{-10} M_{\text{CO}} c^2$ and the radius is normalized by the Schwarzschild radius of the SMBH r_s . The upper panel shows the positive torques, which drive the COs outward, while the lower panel shows the negative ones, which drive the COs closer to the SMBH. The dashed vertical lines mark the locations where a torque changes sign. In this example the parameters are set to $M_{\text{CO}} = 10 M_{\odot}$, $M_{\text{SMBH}} = 10^9 M_{\odot}$, $\dot{M} = 1\dot{M}_{\text{crit}}$ and $\alpha = 0.01$.

gration trap because the driving force is the headwind/tailwind from the non-Kepler disc. It is also different from the stalling mechanism found by Chakrabarti (1993); Molteni et al. (1994), because they considered a balance between the GW torque and the torque due to tailwind, but here we find that the GW torque is much weaker than those due to headwind/tailwind. Most importantly, inside the radius of $r \approx 7 r_s$ there is no more place where the total torque changes sign. So the location $r \approx 7 r_s$ is indeed “the last migration trap”.

To find out whether the last migration trap exists in other cases, we run a grid of calculations with $M_{\text{SMBH}} = 10^7 \sim 10^9 M_{\odot}$, $\dot{M} = 0.1 \sim 10 \dot{M}_{\text{crit}}$, $M_{\text{CO}} = 1 \sim 100 M_{\odot}$ and $\alpha = 0.01 \sim 0.1$. We do not consider those AGNs with higher masses and accretion rates, or the COs with lower masses, because they are rare (Shankar et al. 2009; Woo & Urry 2002; Özel & Freire 2016). Figure 4 shows the parameter space where the last migration trap exists. The calculation is done assuming that $\dot{M} = \dot{M}_{\text{crit}}$ and $\alpha = 0.01$. The location of the migration trap is found at the radius which satisfies two conditions: (i) the migration time-scale is the longest and (ii) the migration time-scale is also longer than 10^7 years, the typical lifetime of AGN. The numbers shown in the figure indicate the radii of the migration traps. We find that larger M_{SMBH} and smaller M_{CO} are more likely to produce migration traps. The trapping radius is small, between 5 and 8 Schwarzschild radii of the central SMBH, which is relatively close to the ISCO ($3 r_s$). In the purple region (upper-left) of the figure, the criteria shown in Equation (18) are met so that a gap would form around the CO. Type II migration would drive the COs to the ISCO and flush them into the SMBH. The green stripe along

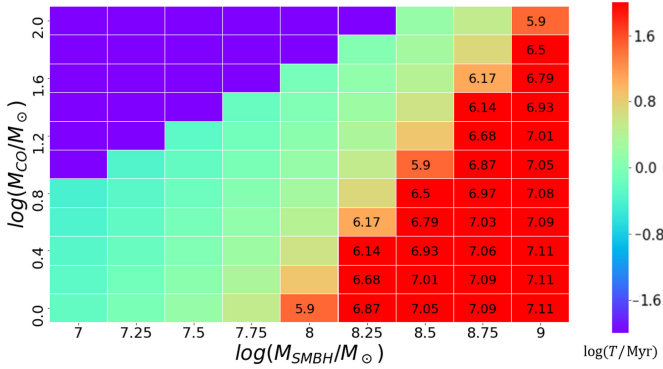


Figure 4. Dependence of the migration time-scale (color coded) on the masses of the SMBH (M_{SMBH}) and the CO (M_{CO}). The other parameters are $\dot{M} = \dot{M}_{\text{crit}}$ and $\alpha = 0.01$. Migration trap is where the migration time-scale is the longest and, at the same time, longer than the typical AGN lifetime, $T_{\text{AGN}} = 10^7$ yrs, and in this case the radius of the trap is shown by the black number (in unit of r_s). The purple region shows the cases where the gap opening criteria in Equation (18) are satisfied.

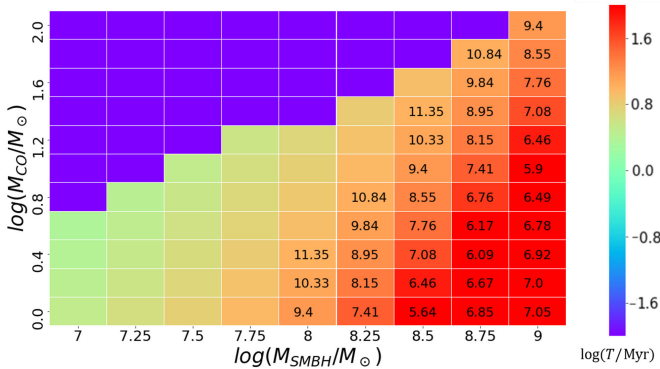


Figure 5. Same as Figure 4 but for $\alpha = 0.1$.

the diagonal is the region where GW radiation is efficient and can flush the COs into the central SMBH.

If we increase the viscosity parameter to 0.1, the major change of the disc is that the gas density drops since the advection velocity increases. As a result, the migration time-scales related to type I and headwind/tailwind both elongate. COs can now spend more time in the accretion disc, so that a larger parameters space could host migration traps, as is shown in Figure 5.

We also studied the dependence of the location of the last migration trap on the accretion rate of the AGN disc. The result is shown in Figure 6. We find that higher accretion rate generally makes the last migration trap more common in AGNs, and the location is pushed closer to the central SMBH. Meanwhile, lower accretion rate suppresses the occurrence of the last migration trap because the headwind/tailwind become weaker. These behaviors can be understood in the context of the strength of the tailwind and its balance with the GW torque.

4 DISCUSSION

In this work, we have studied the migration of the COs embedded in a slim disc around a SMBH. Such discs are expected to form in the most luminous quasars. We paid particular attention to the non-Kepler motion of the gas in the disc and its effect on the COs. We find that such a disc could cause the COs to migrate to a place close to the ISCO where the rotation velocity of the gas transforms from sub-Keplerian to super-Keplerian, and, more importantly, trap the COs there for as long as the lifetime of the accretion disc. We call this place the “last migration trap” because inside it COs can no longer stay for a longtime due to GW radiation.

Our results suggest that the last migration trap is more common in AGNs with heavier SMBHs ($\gtrsim 10^8 M_\odot$) and higher accretion rates ($\dot{M} \gtrsim 0.1 \dot{M}_{\text{crit}}$), and it traps more easily for lighter COs. Take stellar-mass BHs with a mass of $10 M_\odot$ for example, we find that the corresponding last migration trap exists when the SMBH is heavier than $3 \times 10^8 M_\odot$ and the accretion rate is higher than $1 M_{\text{crit}}$, or when the SMBH is heavier than $10^9 M_\odot$ and the accretion rate is higher than $0.1 M_{\text{crit}}$. These requirements for the central SMBH are characteristically different from those derived in the earlier works of Chakrabarti (1993); Molteni et al. (1994); Chakrabarti (1996, 2000); Basu & Chakrabarti (2008), where they found that the migration trap exists even when $M_{\text{SMBH}} = 10^7 M_\odot$ or $M_{\text{CO}} = 10^3 M_\odot$. The discrepancy is caused by the fact that the earlier works assumed a large angular momentum for the gas close to the ISCO, while in our work we computed the angular momentum from a self-consistent accretion disc model. It is worth noting that since the central SMBH is massive when the last migration trap exists, the orbital motion of the trapped COs are generating GWs in a frequency band much lower than 10^{-3} Hz. Such a GW signal cannot be detected by the planned Laser Interferometer Space Antenna (Amaro-Seoane et al. 2017).

The exact locations of the last migration traps can be found in Figures 4, 5 and 6. In other cases, the last migration trap does not exist because the tailwind on the CO, generated by the super-Keplerian inner disc, is too weak to counter the inward migration caused by GW radiation. In these cases where the last migration trap does not exist, we arrive at the same conclusion as in Pan & Yang (2021) that the COs in AGN discs would be flushed to the ISCO and subsequently fall into the central SMBH, though our disc model is different from that in the previous work and we included the mini disc around the CO in the calculation of the drag force.

The presence of a mini disc is a key assumption in our model and hence deserves some discussion. Although it is well accepted that mini discs exist in those two-body systems undergoing mass transfer, such as X-ray binaries (Lin & Pringle 1976; Artymowicz & Lubow 1994), it is unclear whether the mini disc still exists around a CO embedded in the slim disc of an AGN. Our assumption of the mini disc is based on the previous studies on protoplanetary discs. Recent numerical simulations of protoplanetary discs show that mini discs can form around planetesimals (e.g. Machida 2009). In particular, Ormel et al. (2015a) and Ormel et al. (2015b) have shown that mini discs can form in both the wind-dominated and shear-dominated regimes, which correspond to the scenarios depicted, respectively, by the left and right panels of Figure 2. The size of the mini disc around a planetesimal is of the order of the Hills radius (e.g. Fung et al. 2015). However, we note that slim discs have different geometries and thermal-dynamical properties relative to planetary discs. Numerical simulations are needed to elucidate the structure of the gas flow around the COs embedded in slim discs.

In our model, although a large amount of gas will interact with

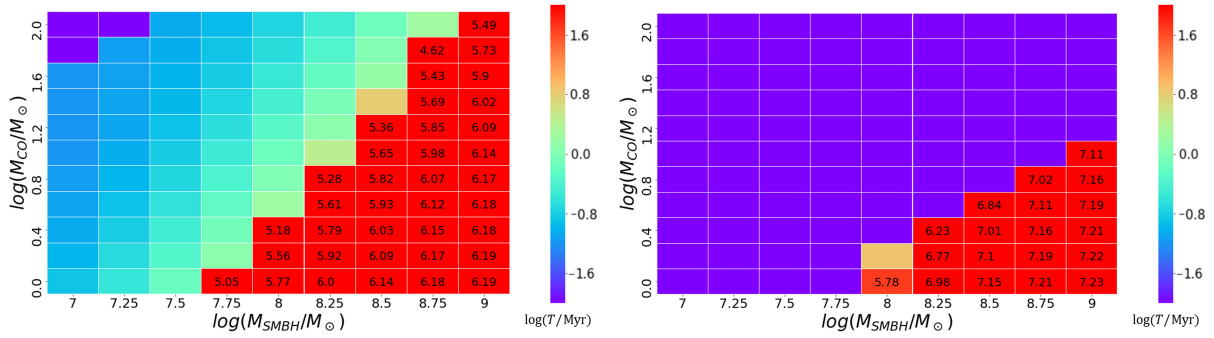


Figure 6. Same as Figure 4, but for $\dot{M} = 10\dot{M}_{\text{crit}}$ (left panel) and $\dot{M} = 0.1\dot{M}_{\text{crit}}$ (right panel).

the mini disc, the mass of the disc is assumed to be constant. This assumption is based on the observation that numerical simulations often show strong outflows from the mini discs (e.g. Tanigawa et al. 2012; Fung et al. 2015; Ormel et al. 2015a,b). One can also compare the internal energy of the gas and the gravitational potential of the CO. The specific internal energy of gas after collision is $(c_s^2 + v_{\text{rel}}^2)/2$, where the second term comes from the kinetic energy of gas before collision. The gravitational potential energy at the edge of the mini disc is GM_{CO}/R_H . Similar to the analysis for Equation 1, we find that the internal energy is larger. Since the internal energy is larger than the potential energy, the gas tends to flow out of the potential of the CO rather than being accreted. Moreover, we assume that the outflow is isotropic so that there is no net force on the mini disc as the gas flows away. The validity of this assumption need to be checked in future numerical simulations. Nevertheless, the details of the outflow would include an extra factor in the expression for the drag force. This factor should be of order unity, unless the effect of outflow somehow cancels out precisely the effect of collision which is unlikely.

Now we estimate the BBH merger rate contributed by the BHs in the last migration trap. The relevant SMBHs are in the mass range of $10^8 - 10^9 M_{\odot}$ and have an accretion rate higher than $0.1\dot{M}_{\text{crit}}$. Further taking into account the fact that LIGO/Virgo only detect the BBHs within a redshift of $z \approx 1$, we find that the number density of the quasars which satisfy the above constraints is $n_{\text{quasars}} = 10^{-7} \text{Mpc}^{-3}$ (Kelly et al. 2009; Vestergaard & Osmer 2009). For each quasar, we following the result of (Tagawa et al. 2020) and assume that a number of

$$N_{\text{BH}} = 3 \times 10^4 \left(\frac{M_{\text{SMBH}}}{10^8 M_{\odot}} \right)^{0.827} \left(\frac{\dot{M}}{\dot{M}_{\text{crit}}} \right)^{1/2} \quad (19)$$

of stellar-mass BHs are captured by the accretion disc. These BHs initially form in the nuclear star cluster, within a distance comparable to the size of the accretion disc from the central SMBH. Tagawa et al. (2020) showed that the BHs in the accretion disc can effectively migrate inward and Pan & Yang (2021) further showed that they would not be trapped by the type I migration trap. Therefore, we assume that the majority of these BHs could reach the last migration trap and form BBHs. With these consideration and typical parameter $M_{\text{SMBH}} = 3 \times 10^8 M_{\odot}$, $\dot{M} = \dot{M}_{\text{crit}}$, we estimate that the event rate is

$$R = \frac{1}{2} n_{\text{quasars}} N_{\text{BH}} / T_{\text{AGN}} \sim 0.4 \text{Gpc}^{-3} \text{yr}^{-1}, \quad (20)$$

where we have assumed a typical lifetime of $T_{\text{AGN}} = 10^7$ yrs for a quasar. We note that this event rate is much higher than the merger rate from another channel, i.e., tidal capture of BBHs by the SMBHs

in gas poor galactic nuclei (Chen & Han 2018). Therefore, the last migration trap is the dominant channel of producing BBH mergers in the vicinity of SMBHs.

The event rate is relatively low compared to the BBH merger rate inferred from the current LIGO/Virgo events. In fact it is about 1 per cent of the rate inferred from LIGO/Virgo observations. Therefore, it is unlikely that all LIGO/Virgo BBHs are produced in the last migration traps. However, as the number of events in the O3 observing run reaches 80 – 90 (Abbott et al. 2020a), the chance of detecting one such event becomes considerably high.

In fact, one LIGO/Virgo event, namely GW190521 (Abbott et al. 2020b), is reported to coincident with an AGN flare and hence may be produced inside the accretion disc of the AGN (Graham et al. 2020), although alternative interpretation of the AGN flare also exists (e.g. De Paolis et al. 2020). GW190521 is also the most massive BBH detected so far, whose BH masses prior to the merger appear to be $66 M_{\odot}$ and $85 M_{\odot}$. Interesting, the luminosity distance of the AGN, $d_{\text{AGN}} \approx 2.2$ Gpc, does not match the apparent distance inferred from the GW signal, $d_{\text{GW}} \approx 4.5$ Gpc. For others, such a discrepancy would refute the association between the AGN and GW190521. For us, however, the discrepancy can be explained using the Doppler and gravitational redshift around the SMBH. Chen et al. (2019) showed that the above two distances are not identical but related as $d_{\text{GW}}/d_{\text{AGN}} = 1 + z$ if Doppler and gravitational redshifts are important. At the ISCO, the total effect of the aforementioned two redshifts ($1 + z$) is between 1.9 and 3.4, depending on the spin parameter of the SMBH. Such a value explains well the different between d_{AGN} and d_{GW} . If GW190521 is indeed produced in the last migration trap, the Doppler and gravitational redshifts could increase the apparent mass by a factor of $d_{\text{GW}}/d_{\text{AGN}} \approx 2$ according to the theory laid out in Chen et al. (2019). Consequently, the real masses of the BHs would be lowered to $(30 - 40) M_{\odot}$. Such smaller BH masses would greatly ease the tension between GW190521 and the theoretical upper limit for the BHs produced by stellar evolution (Woosley 2017).

The existence of the last migration trap also has important implication for the SMBHs in normal galaxies. For example, the center of M87 harbors a SMBH with a mass of $6.5 \times 10^9 M_{\odot}$ (Event Horizon Telescope Collaboration et al. 2019). Its accretion rate is less than $10^{-5} \dot{M}_{\text{crit}}$ (Event Horizon Telescope Collaboration et al. 2021), but in the past the accretion rate should be much higher, probably approaching the Eddington limit, so that the SMBH could grow within a Hubble time to the current mass. During such an active phase, the AGN was likely to have a last migration trap given the large mass of the SMBH. The trap should have created a swamp of BHs in the vicinity of the SMBH. According to Equation (19),

the number of BHs can reach 4×10^5 assuming $\dot{M} = 0.1\dot{M}_{\text{crit}}$. Their mutual interaction could have produced many BBHs through the mechanism presented in Secunda et al. (2019); Tagawa et al. (2020). If some BBHs survive till today, given the closeness of M87 whose distance is about 17 Mpc (Cantiello et al. 2018), they may be detectable by LISA which is more sensitive to long-living BBHs than LIGO/Virgo.

If some BBHs in the LIGO/Virgo band are produced in the last migration trap, it is important to find a way of identifying them. The current difficulty lies in the shortness of the signal in the LIGO/Virgo band, which is normally less than a second. During such a short time span, the acceleration of the center-of-mass of the source, which is often considered as a smoking-gun evidence of a nearby SMBH (e.g. Bonvin et al. 2017; Inayoshi et al. 2017; Meiron et al. 2017), is too weak to be discernible in the waveform. However, recent theoretical works showed that the high velocity of the BBH around the SMBH (Torres-Orjuela et al. 2019, 2020b,a) could induce additional modes to the GW radiation. A possible strong lensing by the SMBH (Kocsis 2013; D’Orazio & Loeb 2020) may also produce distinguishable signatures in the waveform (Dai & Venumadhav 2017; Wang et al. 2021; Ezquiaga et al. 2021). Systematic search in the LIGO/Virgo data for these predicted signatures will help elucidate the importance of this channel of forming BBHs in the last migration trap.

ACKNOWLEDGEMENTS

This work is supported by NSFC grants No. 11873022 and 11991053. X.C. is supported partly by the Strategic Priority Research Program “Multi-wavelength gravitational wave universe” of the Chinese Academy of Sciences (No. XDB23040100 and XDB23010200). The computation in this work was performed on the High Performance Computing Platform of the Centre for Life Science, Peking University.

REFERENCES

Abbott B. P., et al., 2016, *ApJ*, 818, L22
 Abbott B. P., et al., 2020a, *Living Reviews in Relativity*, 23, 3
 Abbott R., et al., 2020b, *Phys. Rev. Lett.*, 125, 101102
 Abbott R., et al., 2020c, *ApJ*, 900, L13
 Abramowicz M., Jaroszynski M., Sikora M., 1978, *A&A*, 63, 221
 Abramowicz M. A., Czerny B., Lasota J. P., Szuszkiewicz E., 1988, *ApJ*, 332, 646
 Abramowicz M. A., Chen X. M., Granath M., Lasota J. P., 1996, *ApJ*, 471, 762
 Abramowicz M. A., Lanza A., Percival M. J., 1997, *ApJ*, 479, 179
 Adachi I., Hayashi C., Nakazawa K., 1976, *Progress of Theoretical Physics*, 56, 1756
 Addison E., Laguna P., Larson S., 2015, preprint, ([arXiv:1501.07856](https://arxiv.org/abs/1501.07856))
 Amaro-Seoane P., et al., 2017, preprint, ([arXiv:1702.00786](https://arxiv.org/abs/1702.00786))
 Antoni A., MacLeod M., Ramirez-Ruiz E., 2019, *ApJ*, 884, 22
 Antonini F., Murray N., Mikkola S., 2014, *ApJ*, 781, 45
 Armitage P. J., 2010, *Astrophysics of Planet Formation*
 Artymowicz P., Lubow S. H., 1994, *ApJ*, 421, 651
 Artymowicz P., Lin D. N. C., Wampler E. J., 1993, *ApJ*, 409, 592
 Barausse E., Cardoso V., Pani P., 2014, *Phys. Rev. D*, 89, 104059
 Bartos I., Kocsis B., Haiman Z., Márka S., 2017, *ApJ*, 835, 165
 Baruteau C., Cuadra J., Lin D. N. C., 2011, *ApJ*, 726, 28
 Basu P., Chakrabarti S. K., 2008, in Chakrabarti S. K., Majumdar A. S., eds, *American Institute of Physics Conference Series Vol. 1053*, American Institute of Physics Conference Series. pp 33–37, doi:10.1063/1.3009504

Bellovary J. M., Mac Low M.-M., McKernan B., Ford K. E. S., 2016, *ApJ*, 819, L17
 Beloborodov A. M., 1998, *MNRAS*, 297, 739
 Bonvin C., Caprini C., Sturani R., Tamanini N., 2017, *Phys. Rev. D*, 95, 044029
 Broadhurst T., Diego J. M., Smoot George I., 2018, arXiv e-prints, p. [arXiv:1802.05273](https://arxiv.org/abs/1802.05273)
 Bryden G., Chen X., Lin D. N. C., Nelson R. P., Papaloizou J. C. B., 1999, *ApJ*, 514, 344
 Cantiello M., et al., 2018, *ApJ*, 856, 126
 Caplar N., Lilly S. J., Trakhtenbrot B., 2017, *ApJ*, 834, 111
 Chakrabarti S. K., 1993, *ApJ*, 411, 610
 Chakrabarti S. K., 1996, *Phys. Rev. D*, 53, 2901
 Chakrabarti S. K., 2000, arXiv e-prints, pp astro-ph/0012529
 Chen X., 2020, arXiv e-prints, p. [arXiv:2009.07626](https://arxiv.org/abs/2009.07626)
 Chen X., Han W.-B., 2018, *Communications Physics*, 1, 53
 Chen X., Li S., Cao Z., 2019, *MNRAS*, 485, L141
 Chen X., Lin D. N. C., Zhang X., 2020, *ApJ*, 893, L15
 Corral-Santana J. M., Casares J., Muñoz-Darias T., Bauer F. E., Martínez-Pais I. G., Russell D. M., 2016, *A&A*, 587, A61
 D’Orazio D. J., Loeb A., 2020, *Phys. Rev. D*, 101, 083031
 Dai L., Venumadhav T., 2017, arXiv e-prints, p. [arXiv:1702.04724](https://arxiv.org/abs/1702.04724)
 Davies M. B., Lin D. N. C., 2020, *MNRAS*, 498, 3452
 De Paolis F., Nucita A. A., Strafella F., Licchelli D., Ingrassio G., 2020, *MNRAS*, 499, L87
 Event Horizon Telescope Collaboration et al., 2019, *ApJ*, 875, L1
 Event Horizon Telescope Collaboration et al., 2021, *ApJ*, 910, L13
 Ezquiaga J. M., Holz D. E., Hu W., Lagos M., Wald R. M., 2021, *Phys. Rev. D*, 103, 064047
 Fung J., Artymowicz P., Wu Y., 2015, *ApJ*, 811, 101
 Gabor J. M., Bournaud F., 2013, *MNRAS*, 434, 606
 Goldreich P., Tremaine S., 1979, *ApJ*, 233, 857
 Goldreich P., Tremaine S., 1980, *ApJ*, 241, 425
 Gonçalves T. S., Steidel C. C., Pettini M., 2008, *ApJ*, 676, 816
 Goodman J., Tan J. C., 2004, *ApJ*, 608, 108
 Graham M. J., et al., 2020, *Phys. Rev. Lett.*, 124, 251102
 Gröbner M., Ishibashi W., Tiwari S., Haney M., Jetzer P., 2020, *A&A*, 638, A119
 Hannuksela O. A., Haris K., Ng K. K. Y., Kumar S., Mehta A. K., Keitel D., Li T. G. F., Ajith P., 2019, *The Astrophysical Journal*, 874, L2
 Hopkins P. F., Hernquist L., 2009, *ApJ*, 698, 1550
 Inayoshi K., Tamanini N., Caprini C., Haiman Z., 2017, *Phys. Rev. D*, 96, 063014
 Kato S., Fukue J., Mineshige S., 2008, *Black-Hole Accretion Disks — Towards a New Paradigm —*
 Kelly B. C., Vestergaard M., Fan X., 2009, *ApJ*, 692, 1388
 Kocsis B., 2013, *ApJ*, 763, 122
 Kolykhalov P. I., Syunyaev R. A., 1980, *Soviet Astronomy Letters*, 6, 357
 LIGO Scientific Collaboration Virgo Collaboration 2019, *Physical Review X*, 9, 031040
 Lančová D., et al., 2019, *ApJ*, 884, L37
 Leigh N. W. C., et al., 2018, *MNRAS*, 474, 5672
 Levin Y., 2007, *MNRAS*, 374, 515
 Lin D. N. C., Papaloizou J., 1986, *ApJ*, 309, 846
 Lin D. N. C., Pringle J. E., 1976, in Eggleton P., Mitton S., Whelan J., eds, Vol. 73, *Structure and Evolution of Close Binary Systems*. p. 237
 MacLeod M., Lin D. N. C., 2020, *ApJ*, 889, 94
 Machida M. N., 2009, *MNRAS*, 392, 514
 McClintock J. E., Narayan R., Steiner J. F., 2014, *Space Sci. Rev.*, 183, 295
 McKernan B., Ford K. E. S., Lyra W., Perets H. B., 2012, *MNRAS*, 425, 460
 McKernan B., et al., 2018, *The Astrophysical Journal*, 866, 66
 Meiron Y., Kocsis B., Loeb A., 2017, *ApJ*, 834, 200
 Molteni D., Gerardi G., Chakrabarti S. K., 1994, *ApJ*, 436, 249
 Norman C., Silk J., 1983, *ApJ*, 266, 502
 Novikov I. D., Thorne K. S., 1973, in *Black Holes (Les Astres Occlus)*. pp 343–450
 Ormel C. W., Kuiper R., Shi J.-M., 2015a, *MNRAS*, 446, 1026

- Ormel C. W., Shi J.-M., Kuiper R., 2015b, *MNRAS*, **447**, 3512
- Özel F., Freire P., 2016, *ARA&A*, **54**, 401
- Paardekooper S. J., Baruteau C., Crida A., Kley W., 2010, *MNRAS*, **401**, 1950
- Pan Z., Yang H., 2021, arXiv e-prints, p. arXiv:2101.09146
- Peters P. C., 1964, *Physical Review*, **136**, 1224
- Sadowski A., 2011, arXiv e-prints, p. arXiv:1108.0396
- Salpeter E. E., 1964, *ApJ*, **140**, 796
- Sartori L. F., et al., 2018, *MNRAS*, **474**, 2444
- Schawinski K., Koss M., Berney S., Sartori L. F., 2015, *MNRAS*, **451**, 2517
- Schutz B. F., 1986, *Nature*, **323**, 310
- Secunda A., Bellovary J., Mac Low M.-M., Ford K. E. S., McKernan B., Leigh N. W. C., Lyra W., Sándor Z., 2019, *ApJ*, **878**, 85
- Secunda A., et al., 2020, *ApJ*, **903**, 133
- Shankar F., Weinberg D. H., Miralda-Escudé J., 2009, *ApJ*, **690**, 20
- Shlosman I., Begelman M. C., 1989, *ApJ*, **341**, 685
- Sądowski A., 2009, *ApJS*, **183**, 171
- Smith G. P., Jauzac M., Veitch J., Farr W. M., Massey R., Richard J., 2018, *MNRAS*, **475**, 3823
- Stone N. C., Metzger B. D., Haiman Z., 2017, *MNRAS*, **464**, 946
- Syer D., Clarke C. J., Rees M. J., 1991, *MNRAS*, **250**, 505
- Tagawa H., Haiman Z., Kocsis B., 2020, *ApJ*, **898**, 25
- Tanigawa T., Ohtsuki K., Machida M. N., 2012, *ApJ*, **747**, 47
- The LIGO Scientific Collaboration et al., 2020, arXiv e-prints, p. arXiv:2010.14533
- Torres-Orjuela A., Chen X., Cao Z., Amaro-Seoane P., Peng P., 2019, *Phys. Rev. D*, **100**, 063012
- Torres-Orjuela A., Chen X., Amaro-Seoane P., 2020a, arXiv e-prints, p. arXiv:2010.15856
- Torres-Orjuela A., Chen X., Amaro-Seoane P., 2020b, *Phys. Rev. D*, **101**, 083028
- Vestergaard M., Osmer P. S., 2009, *ApJ*, **699**, 800
- Wang J.-M., Yan C.-S., Gao H.-Q., Hu C., Li Y.-R., Zhang S., 2010, *ApJ*, **719**, L148
- Wang Y., Lo R. K. L., Li A. K. Y., Chen Y., 2021, arXiv e-prints, p. arXiv:2101.08264
- Ward W. R., 1991, in Lunar and Planetary Science Conference. p. 1463
- Ward W. R., 1997, *Icarus*, **126**, 261
- Weidenschilling S. J., 1977, *MNRAS*, **180**, 57
- Weidenschilling S. J., Cuzzi J. N., 1993, in Levy E. H., Lunine J. I., eds, Protostars and Planets III. p. 1031
- Woo J.-H., Urry C. M., 2002, *ApJ*, **579**, 530
- Woosley S. E., 2017, *ApJ*, **836**, 244
- Yang Y., et al., 2019, *Phys. Rev. Lett.*, **123**, 181101
- Youdin A. N., Shu F. H., 2002, *ApJ*, **580**, 494
- Yunes N., Kocsis B., Loeb A., Haiman Z., 2011, *Phys. Rev. Lett.*, **107**, 171103

This paper has been typeset from a $\text{\TeX}/\text{\LaTeX}$ file prepared by the author.